

# The fulcrum wavelength of young stellar objects - the case of LRL 31

Geoffrey R. Bryan,<sup>1\*</sup> Sarah T. Maddison<sup>1</sup> and Kurt Liffman<sup>1</sup>

<sup>1</sup>Centre for Astrophysics and Supercomputing, Swinburne University of Technology, Hawthorn, Victoria 3018, Australia

Accepted 2019 August 18. Received 2019 August 11; in original form 2019 April 30

## ABSTRACT

A small subset of young stellar objects (YSOs) exhibit “see-saw” temporal variations in their mid-infrared SED; as the flux short-ward of a fulcrum wavelength ( $\lambda_f$ ) increases the flux long-wards of this wavelength decreases (and vice-versa) over timescales of weeks to years. While previous studies have shown that an opaque, axisymmetric occulter of variable height can cause this behaviour in the SED of these objects, the conditions under which a single  $\lambda_f$  occurs have not previously been determined, nor the factors determining its value. Using radiative transfer modelling, we conduct a parametric study of the exemplar of this class, LRL 31 to explore this phenomenon, and confirm that the cause of this flux variation is likely due to the change in height of the optically thick inner rim of the accretion disc at the dust sublimation radius, or some other phenomenon which results in a similar appearance. We also determine that a fulcrum wavelength only occurs for high inclinations, where the line of sight intersects the accretion disc. Accepting that the disc of LRL 31 is highly inclined, the inner rim radius, radial and vertical density profiles are independently varied to gauge what effect this had on  $\lambda_f$  and its position relative to the silicate feature near  $10\mu\text{m}$ . While  $\lambda_f$  is a function of each of these parameters, it is found to be most strongly dependent on the vertical density exponent  $\beta$ . All other factors being held constant, only for flatter discs ( $\beta < 1.2$ ) did we find a  $\lambda_f$  beyond the silicate feature.

**Key words:** SED – radiative transfer modelling – disc structure

## 1 INTRODUCTION

High resolution imaging in the optical and submillimetre provide detailed views of the structure of discs (ALMA Partnership et al. 2015; Ansdell et al. 2016b; Avenhaus et al. 2018), neither of these techniques can currently image the inner few au of nearby young stellar object (YSO) discs where rocky planets are expected to form (Dullemond & Monnier 2010). The spectral energy distribution (SED) of YSOs have been found to vary in the mid-infrared (MIR), suggesting variation in the distribution of gas and dust in the inner planet-forming region of the disc (Muzerolle et al. 2009; Flaherty et al. 2011; Espaillat et al. 2010, 2012).

Infrared space observations have found that a significant proportion of YSOs vary in the MIR on all measured timescales (Cody et al. 2014; Rebull et al. 2015; Flaherty et al. 2016). Between 5-30% of the YSOs are classified as *dippers*, which vary on timescales of the order of days (Bouvier et al. 1999; Morales-Calderón et al. 2011). They exhibit deep, colourless dips in brightness of occasionally more than

a magnitude, and typically with periods similar to the rotation periods of their star. One popular hypothesis to explain this dipping behaviour is that it is caused by the occultation of the central star by a segment of the inner wall of the disc warped out of the plane of rotation by interaction with a strong magnetic field (Lai & Zhang 2008). However, recent studies have cast doubt on whether this can be the full explanation (Ansdell et al. 2016a). Espaillat et al. (2010) uncovered another class of MIR variable YSOs which exhibit aperiodic “see-saw” flux variations. The SEDs of these YSOs have a fulcrum wavelength ( $\lambda_f$ ), about which as the wavelength weighted flux  $\lambda F_\lambda$  increases shortward of  $\lambda_f$ , it simultaneously decreased for wavelengths longward of  $\lambda_f$  and vice-versa. This type of MIR variability is the focus of this paper.

A variety of mechanisms have been proposed by Flaherty et al. (2011) to explain these see-saw like fluctuations in flux. These include: an increased accretion rate resulting in an increase in the scale height of the disc’s inner wall (Dullemond et al. 2001); an increase in disc surface density leading to an increased scale height (D’Alessio et al. 1998); or a stellar wind ablating dust from the disc surface and

\* E-mail: gbryan@swin.edu.au (CAS)

creating an opaque cloud of dust some scale heights high (Flaherty & Muzerolle 2010; Königl et al. 2010). Magnetic fields might warp the inner disc out of the rotation plane (Lai & Zhang 2008) or a small unobserved companion orbiting out of the plane of the disc might drag dust with it (Larwood & Papaloizou 1997). One common factor in all of these scenarios is the presence of an optically thick occulter blocking the observer’s line-of-sight to the star.

Possibly the simplest model is one where there is an inflation and then deflation of an optically thick axisymmetric inner rim located at the dust sublimation radius (Dullemond & Monnier 2010; Dong 2015). The presence of a puffed, opaque rim, or something like it, casting a shadow on the disc external to itself was originally proposed by Natta et al. (2001) and expanded upon by Dullemond et al. (2001) to account for the properties of the SEDs of Herbig Ae/Be stars.

When the opaque inner rim inflates, it casts a shadow on the disc radially exterior to it. The region in the shadow will then cool rapidly to the ambient temperature of the stellar environment (typically to tens of degrees Kelvin), provided we ignore the effects of thermal diffusion from the regions still illuminated. At the same time, for all but a face-on presentation of the system, the apparent height of the illuminated inner rim increases and the amount of shortwave flux will increase linearly as a function of the rim height. Thus, the result of the disc puffing is to cause a pivot in the SED with an increase in the shortwave flux and a decrease in the longwave flux emitted by the object. While this model does explain the temporal see-saw variation in the SEDs of these YSOs, it does not explain the presence of a unique  $\lambda_f$  for these systems.

This paper seeks to determine what additional factors must be taken into account to yield a unique  $\lambda_f$  for systems exhibiting this temporal see-saw behaviour in the MIR and which of these parameters most strongly determines its value. We consider the exemplar of the class of see-saw variables, LRL 31, to study this phenomenon.

## 2 METHODS

We use the Monte Carlo radiative transfer code Hochunk3D (Whitney et al. 2003c,a, 2013) to model the SED of cTTs to explore key parameters that could cause the see-saw variability in the MIR flux. Using a parametric disc model, the code calculates the disc temperature and then the SED. We specify the stellar properties of LRL 31 (mass, radius and effective temperature), plus the geometry and material properties of the accretion disc. We use a cylindrical-polar mesh with a logarithmic distribution of cell sizes in the radial direction. A Planck blackbody curve (with limb darkening) is used to model the stellar source. In our simulations we specify a disc accretion rate,  $\dot{M}_{\text{disc}}$ , instead of a fixed viscosity parameter,  $\alpha$ , as an accretion rate can be directly derived from observations of the Brackett and Paschen absorption lines (Muzerolle et al. 2009), and allow the code to calculate the disc accretion luminosity, which is added to the total calculated luminosity of the disc.

Hochunk3D models the accretion disc as two distinct, inter-penetrating discs which can have different geometric and material properties. In our simulations, we model a thin, settled disc, which contains larger dust particles and a more

extended disc, which contains smaller particles. Both discs are modelled as a mixture of dust and gas, with 20% of the total disc mass comprising the settled disc of larger grains (following the model of Wood et al. (2002)). The remaining 80% of the total disc mass is found in the extended disc with fine grain parameters derived by Kim et al. (1994) from properties of ISM dust.

The disc density,  $\rho$ , is parameterised in Hochunk3D as:

$$\rho(R, z) = \rho_0 \left( 1 - \sqrt{\frac{R_\star}{R}} \right) \left( \frac{R_\star}{R} \right)^\alpha \exp \left\{ -\frac{1}{2} \left[ \frac{z}{h(R)} \right]^2 \right\}. \quad (1)$$

Where the scale height,  $h$ , is given by equation 2

$$h(R) = h_0 \left( \frac{R}{R_\star} \right)^\beta, \quad (2)$$

and where  $R$  and  $z$  are the radial and vertical cylindrical components,  $R_\star$  the stellar radius,  $\rho_0$  is the local mid-plane density, and  $\alpha$  and  $\beta$  respectively the radial and vertical density profile exponents.

Following the arguments of Lynden-Bell & Pringle (1974) and Pringle (1981), a characteristic length scale in the  $z$ -direction, the isothermal scale height,  $H_{\text{iso}}$  can be derived

$$H_{\text{iso}}(R) = \sqrt{\frac{k_B T_{\text{eff}} R^3}{\bar{m} \mu G M_\star}} = \left( \sqrt{\frac{k_B T_{\text{eff}}}{\bar{m} \mu}} \left| \sqrt{\frac{G M_\star}{R_\star}} \right| \left( \frac{R}{R_\star} \right)^{\frac{3}{2}} \right) R_\star, \quad (3)$$

wherein  $k_B$  is the Boltzmann constant,  $\bar{m}$  the mean molecular mass of the gas,  $\mu$  the atomic mass unit,  $G$  the gravitational constant, and  $T_{\text{eff}}$  and  $M_\star$  the stellar effective temperature and mass.

At the stellar photosphere radius the isothermal scale height is:

$$h_0 = H_{\text{iso}}(R_\star) = \left( \sqrt{\frac{k_B T_{\text{eff}}}{\bar{m} \mu}} \left| \sqrt{\frac{G M_\star}{R_\star}} \right| \right) R_\star \quad (4)$$

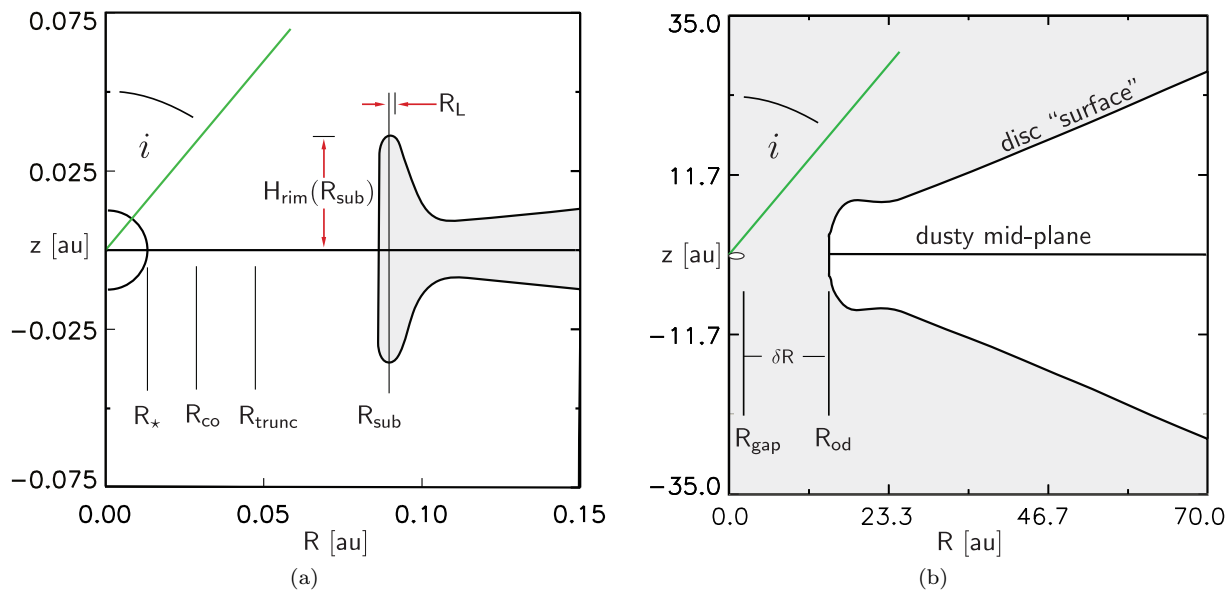
and it is this value that we use to set the value of the constant  $h_0$  in equation 2.

Figure 1(a) illustrates the geometry of the inner region of the LRL 31 system. The primary geometric properties are the radius of the star  $R_\star$ , the dust sublimation radius  $R_{\text{sub}}$ , the co-rotation radius  $R_{\text{co}}$ , and the disc truncation radius  $R_{\text{trunc}}$ . In the outer region of the disc (Figure 1(b)) the relevant geometric quantities are: the radius to the edge of the inner disc gap  $R_{\text{gap}}$ , the gap width  $\delta R$ , and the radial position of the inner rim of the outer disc  $R_{\text{od}}$ . The inclination of the disc to the observer is denoted by  $i$ .

The dust sublimation radius  $R_{\text{sub}}$  is set by the dust sublimation temperature  $T_{\text{sub}}$  for silicates ( $\sim 1,500$  K), and material interior to  $R_{\text{sub}}$  is assumed to be optically thin. Just beyond  $R_{\text{sub}}$  dust will condense, forming the inner wall of the accretion disc. Heating of the inner wall by stellar irradiation is thought to puff the inner rim,  $H_{\text{rim}}$ , by some factor greater than unity of the isothermal scale height and also potentially increase the inner rim length in the radial direction,  $R_L$ .

Using a slight modification of the Stefan-Boltzmann relation due to Whitney et al. (2004), the dust sublimation radius of LRL 31 can be estimated:

$$R_{\text{sub}} = \left( \frac{T_{\text{eff}}}{T_{\text{sub}}} \right)^{2.1} R_\star. \quad (5)$$



**Figure 1.** Schematics of the geometry of LRL 31 disc. (a) Inner disc showing the puffed inner rim ( $R_{\text{co}}$  and  $R_{\text{trunc}}$  not to scale); and (b) outer disc with a gap of width  $\delta R$ .

**Table 1.** Properties of LRL 31.

Parameter	Description	Value	References
SpType	Spectral type	G6V	[1]
$M_{\star}$	Mass	$1.6 M_{\odot}$	[2], [3]
$T_{\text{eff}}$	Temperature	5,700 K	[2], [6]
$R_{\star}$	Radius	$2.3 R_{\odot}$	[2]
$L_{\star}$	Luminosity	$5 L_{\odot}$	[2]
$P_{\star}$	Rotational period	3.4 days	[2]
$B_{\star}$	Magnetic field strength	0.15 T	[4]
$d$	Distance	315 pc	[5], [7]
$A_{\text{v}}$	Extinction	$\sim 8.3$	[1]

[1] Muzerolle et al. (2009), [2] Flaherty et al. (2011), [3] Espaillat et al. (2012), [4] Liffman et al. (2019), [5] Pinilla et al. (2014), [6] Kenyon & Hartmann (1995), [7] Luhman et al. (2003)

For  $T_{\text{sub}} \approx 1,500$  K,  $R_{\text{sub}} = 16.5R_{\star}$  and the orbital period at that distance is  $P = 21.3$ d. This sets a natural time scale for the inner regions of the system: of the order of days to weeks.

Parameters which could vary on timescales of days and weeks and result in fluctuations in the MIR SED on similar timescales include the disc accretion rate,  $\dot{M}_{\text{disc}}$ , and the inner rim height  $H_{\text{rim}}$ .

## 2.1 Modelling the exemplar - LRL 31

The exemplar of these see-saw variable YSOs is LRL 31, located in the nebula IC348 of the Perseus star-forming region in Perseus. IC348 is approximately 315 pc from the Sun and contains a young stellar cluster approximately 2 million years old. LRL 31 is of spectral type G6V. LRL 31 has been observed by multiple observers with the *Spitzer Space Telescope* (Muzerolle et al. 2009; Flaherty et al. 2011). Radiative transfer modelling by Espaillat et al. (2012) suggests

**Table 2.** Characteristics of the LRL 31 accretion disc.

Parameter	Description	Value	References
$\dot{M}_{\text{disc}}$	Accretion rate	$0.25 - 3.32 \times 10^{-8} M_{\odot} \text{yr}^{-1}$	[1], [2]
$M_{\text{disc}}$	Disc mass	$< 0.06 M_{\odot}$	[4]
$R_{\text{disc}}$	Maximum disc radius	300 au	[4]
$R_{\text{trunc}}$	Truncation radius	$5 R_{\odot}$	[5]
$\bar{m}$	Mean molecular mass	2.3 amu	
$i$	Inclination	$> 70^{\circ}$	[3]

[1] Muzerolle et al. (2009), [2] Flaherty et al. (2011), [3] Flaherty & Muzerolle (2010), [4] Espaillat et al. (2012), [5] Liffman et al. (2019)

**Table 3.** Additional parameters in the fiducial model of LRL 31.

Parameter	Description	Value
$\alpha$	radial density exponent	2.25
$\beta$	vertical density exponent	1.25
$H_{\text{puff}}$	Additive rim puffing factor	0.0
$R_{\text{L}}$	Inner rim length	0.01 au
$\delta R$	Disc gap width	0.0 au
FDISK	$M_{\text{settled}}/M_{\text{disc}}$	0.2

it is a pre-transition disc with a gap in its disc of width 14 au. Muzerolle et al. (2009) found significant infrared variability on time-scales as short as a week, with the SED pivoting about  $\lambda_f = 8.5 \mu\text{m}$ .

Unless otherwise explicitly noted, we use disc properties derived from observations reported in Muzerolle et al. (2009); Flaherty & Muzerolle (2010) and Flaherty et al. (2011) as the basis for our fiducial simulation.

Given our primary goal is to test for the key parameters

that could result in a fulcrum in the SED of LRL 31, rather than try to determine the best model fit for the SED, we have made a number of simplifying assumptions in our fiducial model.

We assumed that the occulter (an opaque inner rim wall or some other object) is axisymmetric.

We assume that the central star is a blackbody with  $T_{\text{eff}} = 5,700$  K and spectral type G6V. While the code does allow for more accurate stellar atmosphere models, our aim here is to test a relatively simple geometric model rather than make absolutely accurate predictions of the SED of LRL 31.

Unpublished observations in the *I* band by N. Baliber et al. (Flaherty et al. 2011) show small variations in the flux which are hypothesised to be due to the rotation of cool spots across the stellar surface, which suggest that the rotational period of the star is approximately 3.4 days. The co-rotation radius,  $R_{\text{co}}$ , is the radius at which the orbital period matches the rotation period of the star at its equator, which for LRL 31 it is at approximately 0.03 au.

Magnetic field strengths around cTTs have been deduced to be approximately 1 kG (Bouvier et al. 2007). The truncation radius,  $R_{\text{trunc}}$ , demarcates the edge of the magnetospheric cavity at which position the ram pressure of the disc material exceeds the support provided by the magnetic pressure. At  $R_{\text{trunc}}$  the disc terminates and the disc material accretes directly onto the surface of the star in accretion columns. For LRL 31, adopting  $B \approx 1.5$  kG and  $\dot{M}_{\text{disc}} = 1.6 \times 10^{-8} M_{\odot} \text{yr}^{-1}$ , Liffman et al. (2019) calculated  $R_{\text{trunc}} \approx 0.13$  au.

Espaillet et al. (2012) observed millimetre fluxes from LRL 31 and following Beckwith et al. (1990) and Beckwith & Sargent (1991) were able to calculate an upper bound on the disc mass of  $M_{\text{disc}} < 0.06 M_{\odot}$ . We, however, adopt a lower value of  $M_{\star} = 0.01 M_{\odot}$ . We also adopt  $R_{\text{disc}} = 300$  au used by Espaillet et al. (2012) in their radiative transfer simulations.

LRL 31 is a pre-transition object with at least one disc gap occurring between 1 and 15 au (Espaillet et al. 2012; Pinilla et al. 2014). However, for the sake of simplicity, our initial model assumes no gap. We will see the effect of the gap in our latter model.

Over the two years post December 2007, the extinction  $A_V$  of LRL 31 was observed by Flaherty et al. (2011) to vary between 8.1 to 9.2 with an average at  $A_V \sim 8.3$ , while the polarisation was observed to vary between 7.70% and 8.44%. The values of the polarization are high compared to other nearby cTTS and indicate that some portion of the stellar light passed through the bulk of the disc, suggesting that it is highly inclined to the observer. Following this reasoning Flaherty & Muzerolle (2010) adopted a value of  $i = 85^\circ$ . Previously, Muzerolle et al. (2009) had also adopted a near edge on orientation for the object. For this study, we assume only that the disc inclination  $i > 70^\circ$ , but for each Hochunk3D simulation run we sweep through 90 values of the inclination, equi-spaced in  $\cos(i)$  between  $6.0^\circ$  and  $89.7^\circ$  so as to observe the full effect of varying disc inclination.

Accretion rates for LRL 31 were deduced from observations of the Pa $\beta$  and the Bry lines by Flaherty et al. (2011). The line luminosities had been shown to be directly correlated with the accretion luminosity (Muzerolle et al.

1998) via:

$$L_{\text{acc}} = \frac{3G\dot{M}_{\text{disc}}M_{\star}}{5R_{\star}}. \quad (6)$$

Over 9 epochs of observation between October 2008 and November 2009,  $\dot{M}_{\text{disc}}$  varied between 0.25 and  $3.32 \times 10^{-8} M_{\odot} \text{yr}^{-1}$ . As the fiducial value of the accretion rate we chose  $1.60 \times 10^{-8} M_{\odot} \text{yr}^{-1}$  (which occurred on the 8<sup>th</sup> November 2008) as a value between the ends of this range.

Flaherty et al. (2011) subtracted the spectrum of the Type G6, WTTS HD 283572 augmented by a Kurucz model ( $T_{\text{eff}} = 5,750$ ,  $\log g = 2.5$ ) and reddened to  $A_V = 8.2$  to determine the infrared excess due to the supposed puffed inner rim of LRL 31. Working on the assumption that the inner rim is optically thick (and so can be accurately approximated by a single temperature blackbody), they fitted the infrared excess to determine the temperature of the inner rim and the covering fraction of the star. Based on observations over 11 nights between 2005 and 2009 they deduced that  $1,540 < T_{\text{rim}} < 1,940$  K, with an average of  $T_{\text{rim}} = 1,830$  K. This is considerably higher than the dust sublimation temperature ( $T_{\text{sub}} = 1,500$  K) discussed in Dullemond & Monnier (2010) and is towards the upper end of the temperature range at which refractory dust species sublime. They derived a small, dust sublimation radius of 0.05 au for the highest sublimation temperature and a larger radius of 0.3 au for the lowest dust sublimation temperature. They argued for the feasibility of the higher temperature provided the dust at that radius consists of larger grains (a few  $\mu\text{m}$ ) which can radiate more efficiently at this wavelength range than smaller grains (0.1  $\mu\text{m}$ ). Hochunk 3D does not use  $T_{\text{rim}} = T_{\text{sub}}$  directly as a simulation input, but rather the  $R_{\text{sub}}$  derived from this temperature. We adopt  $T_{\text{sub}} = 1,500$  K as our fiducial value.

If the measured infrared excess is due to stellar flux reprocessed by an opaque inner puffed rim then fluctuations in this flux will be proportional to the covering fraction of the stellar source by the inner disc wall, which in turn is proportional to the puffed inner rim height  $H_{\text{rim}}(R)$ . The flux due to the wall is  $F_{\lambda, \text{rim}}$ , where

$$F_{\lambda, \text{rim}} \approx \frac{4\pi R_{\text{rim}} H_{\text{rim}}(R_{\text{rim}}) B_{\lambda}(T_{\text{rim}})}{d^2} \sin(i). \quad (7)$$

and  $B_{\lambda}(T_{\text{rim}})$  is the value of the Planck function at wavelength  $\lambda$  at the temperature of the rim  $T_{\text{rim}}$ .

Flaherty et al. (2011) has stated that their analysis of the infrared excess shows that  $T_{\text{rim}}$  (and hence  $R_{\text{rim}}$ ) remained approximately constant during their observations. So a change in the infrared excess by a factor of two between 31<sup>st</sup> October and the 4<sup>th</sup> November 2009 is best explained by an increase in a factor of two in the puffed rim height  $H_{\text{rim}}(R_{\text{rim}})$ . The largest increase in value in  $H_{\text{rim}}(R_{\text{rim}})$  was inferred to be a factor of 4 between 8<sup>th</sup> October 2009 and 9<sup>th</sup> November 2009. In our radiative transfer simulations we simulate fluctuations in the inner rim height in the range 1 to 7.5 of the unpuffed rim height.

Unless the accretion disc is particularly massive ( $M_{\text{disc}} > 0.1 M_{\odot}$ ) the contribution to the total luminosity due to viscous dissipation is small (a few percent) and such passive discs flare so that the central star is visible from everywhere on the disc's surface. We adopt the values for the radial exponent  $\alpha$  and the flaring exponent  $\beta$  for a passive, flaring



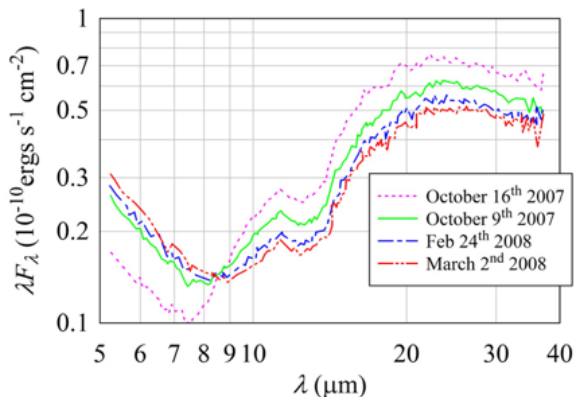


**Figure 2.** The SED of LRL 31, with *Spitzer* IRS data from Flaherty et al. (2011).

disc derived by Kenyon & Hartmann (1987):  $\alpha = 2.25$  and  $\beta = 1.25$ , for our fiducial simulation.

## 2.2 Simulation suite

The stellar and disc parameters of LRL 31 are given in Tables 1 & 2 respectively, with additional parameters using the fiducial model given in Table 3. In our fiducial model  $\dot{M}_{\text{disc}} = 1.60 \times 10^{-8} M_{\odot} \text{yr}^{-1}$  and  $M_{\text{disc}} = 0.01 M_{\odot}$ . For all our simulations, we compare the resulting simulated SEDs with the *Spitzer* IRS data from Flaherty et al. (2012) – see Figure 2. We test for the presence or otherwise of a fulcrum point, the value of  $\lambda_f$ , and the magnitude of the weighted flux  $\lambda F_{\lambda}$ .

### 2.2.1 A puffed inner rim

In our first set of simulations (Sim. 1; Table 4) we vary the puffed inner rim height scale factor,  $H_{\text{puff}}$  and the disc inclination to the line of sight,  $i$ .

Hochunk3D parameterises the puffed inner rim using the expression (Figure 2)

$$H_{\text{rim}}(R) = h(R) \left[ 1 + H_{\text{puff}} \exp \left( - \left( \frac{R - R_{\text{rim}}}{R_L} \right)^2 \right) \right]. \quad (8)$$

Here:  $H_{\text{rim}}(R)$  is the puffed rim height at  $R$ ,  $h(R)$  is the scale height of the unpuffed disc at radius  $R$ ,  $H_{\text{puff}}$  is the puffed inner rim height scale factor and  $R_L$  is the characteristic rim length in the radial direction.  $H_{\text{puff}}$  varies between 0.0 to 6.5 in 10 equal intervals, and for each of these simulations the inclination varies from being almost face-on ( $i = 6^\circ$ ) to almost edge-on ( $i = 87^\circ$ ) on a grid of 90 inclinations equispaced in  $\cos i$  (see Table 4).

### 2.2.2 Varying disc accretion rate, $\dot{M}_{\text{disc}}$

Varying the accretion rate in the inner part of the disc is expected to contribute directly to fluctuations in the flux at short wavelengths in the ultraviolet as well as in the infrared. Observations of LRL 31's veiled Brackett and Paschen lines suggest that it has an irregular accretion rate (Muzerolle et al. 2009; Flaherty et al. 2011).

In our second set of simulations (Sim 2; Table 4); we varied the mass accretion rate between  $1.6 \times 10^{-8} - 1.6 \times 10^{-7}$  in 11 uniform steps while keeping all other parameters of the fiducial model constant.

### 2.2.3 $T_{\text{rim}}$ and the fulcrum wavelength $\lambda_f$

Assuming that  $H_{\text{rim}}$  and/or  $\dot{M}_{\text{disc}}$  are the parameters whose variation results in a single fulcrum point in the MIR SED, we next explored the factor (or factors) which determine the value of  $\lambda_f$ .

Our principal hypothesis was that the stellar temperature is kept fixed, but that the radius of the inner rim of the accretion disc is no longer at the dust sublimation radius, but rather at the much larger radius of the inner disc cavity and that it is the cavity radius which determines  $\lambda_f$ .

As previously noted, for  $R < R_{\text{sub}}$  the material of the disc is likely to be optically thin because it will be above the  $T_{\text{sub}}$ . However, there are many mechanisms (see Koepferl et al. 2013) that can clear material from the inner zone of the disc: the presence of a small companion (Ireland & Kraus 2008), photo-evaporation (Alexander et al. 2006a,b), strong stellar winds (Konigl & Pudritz 2000) or a recent star burst (Ábrahám et al. 2009), eroding the inner edge of the disc and leaving the outer disc intact, where the temperature is lower than  $T_{\text{sub}}$ . To explore this possibility, we ran a suite of simulations where we kept  $T_{\text{eff}} = 5,700$  K (the fiducial value) while varying the inner rim temperature between 1,000–2,000 K. We used the relation equation 5 to calculate the radius at which  $T_{\text{rim}}$  took on these temperatures. For each temperature, 11 simulations were run for puffed inner rim scale factors  $H_{\text{puff}}$  between 0.0 and 6.5 (see Table 5). These simulations mimic the initial set (Sim. 1) in which the inner rim puffs and deflates due to some as yet undetermined cause, but with a different inner rim radius.

### 2.2.4 Modelling the effect of disc structure on the SED and the occurrence of $\lambda_f$

To explore more generally the presence or otherwise of a fulcrum wavelength in LRL 31 and the values it could take, we investigated the effect of changes in other parameters which do not vary on a temporal scale of days or weeks, and which can be expected to be unique to different cTTs. These parameters include: the radial density exponent  $\alpha$  and the disc flaring exponent  $\beta$  and the presence or absence of a gap in the disc.

We explored the effect of varying the radial density exponent,  $\alpha$ , on either side of the fiducial value, [ $2.0 < \alpha < 2.45$ ]. As the discs of cTTs are generally known to flare we selected a range of values for the flaring exponent  $\beta$  in our simulations such that the disc varied between being flat,  $\beta = 1.0$ , and having a slightly more flared profile,  $\beta = 1.30$ , than the fiducial value of  $\beta = 1.25$ . In our simulations  $\alpha$  and  $\beta$  were varied independently.

As our principal aim was to examine what the effect of the gross structure of the disc had on the existence or otherwise of a fulcrum point and on  $\lambda_f$ , the fiducial simulation included no gap. However, it has been deduced that LRL 31 is a transition disc with a 14 au gap in its inner disc. Consequently we have also modelled the SED of LRL 31 where

**Table 4.** Parameters varied in the simulation suite.

Simulation	Parameter	Start value	End value	No. of increments	Increment
Sim. 1	$H_{\text{puff}}$	0.00	6.50	10	0.65
Sim. 2	$\dot{M}_{\text{disc}}(\text{M}_{\odot}\text{yr}^{-1})$	$1.6 \times 10^{-8}$	$1.6 \times 10^{-7}$	10	$1.44 \times 10^{-8}$
Sim. 3	$T_{\text{rim}}(\text{K})$	1,000	2,000	4	250
Sim. 4	$\delta R(\text{au})$	14.0	0	0	0
Sim. 5	$\alpha$	2.0	2.5	5	0.2
Sim. 6	$\beta$	1.0	1.3	6	0.05

**Table 5.** Additional parameters varied in the inner disc rim temperature simulations (Sim. 3),  $T_{\text{eff}} = 5,700$  K.

$T_{\text{rim}}[\text{K}]$	$R_{\text{rim}}[\text{au}]$	$H_{\text{puff}}$
1,000	0.3474	0 – 6.5
1,250	0.2223	0 – 6.5
1,500	0.1544	0 – 6.5
1,750	0.1134	0 – 6.5
2,000	0.0860	0 – 6.5

such a gap is present, varying the puffed inner rim height factor,  $H_{\text{puff}}$  in the range:  $0 < H_{\text{puff}} < 6.5$ .

### 3 RESULTS

#### 3.1 Varying the puffed inner rim scale factor, $H_{\text{puff}}$

We varied the inner rim height over 11 values (Table 4). Figure 3 shows the resulting SEDs for a near face-on disc with  $i = 6.0^\circ$ , where the puffed inner rim height scale factor varied from  $H_{\text{puff}} = 0.0 - 6.5$ . Varying  $H_{\text{rim}}$  results in a see-saw variation in the SED near  $8 \mu\text{m}$ . For increasing  $H_{\text{rim}}$  the flux short-ward of  $8 \mu\text{m}$  increases and the flux long-ward of  $8 \mu\text{m}$  decreases. Note that for this almost face-on presentation, there is no single pivot (or fulcrum) point but rather a series of cross-over points spread between  $7$  and  $15 \mu\text{m}$ . The diagram on the right of Figure 3 shows contour plots of the density of the parametric disc, with the (green) line showing is the line of sight.

As we increase the disc inclination, the magnitude of the photospheric peak decreases while the peak in the SED due to the inner wall of the disc increases in magnitude and becomes prominent. It is only when the line of sight begins to graze the disc surface at  $\approx 75^\circ$  that a single fulcrum wavelength or pivot point appears near  $8 \mu\text{m}$  (Figure 4). As the inclination increases further and the line of sight cuts through the disc, a pivot point is still observed at near  $8 \mu\text{m}$ , though the magnitude of the flux at that point rapidly decreases. For inclinations above  $82^\circ$ , the simulations become increasingly noisy and it is difficult to determine the presence (or otherwise) of a pivot point.

Figure 5 shows the MIR portion of the SED between  $5 \mu\text{m}$  and  $40 \mu\text{m}$ , with  $i = 75^\circ$  - no reddening has been applied during post-processing. The key feature of the plot is the presence of a fulcrum point,  $\lambda_f$ , near  $8 \mu\text{m}$  shortward of the  $10 \mu\text{m}$  silicate feature. This is in general agreement with the LRL 31 SED shown in Figure 2.

#### 3.2 Varying the mass accretion rate, $\dot{M}_{\text{disc}}$

Figure 6 shows the results of simulations which vary the mass accretion rate between  $\dot{M} = 1.6 \times 10^{-8} - 1.16 \times 10^{-7} \text{ M}_{\odot}\text{yr}^{-1}$  for two different inclinations: almost face-on with  $i = 6.0^\circ$ , and almost edge-on with  $i = 83.3^\circ$  in which the line of sight passes through the disc. In both cases, increasing the accretion rate increases the flux without appreciably changing the shape of the SED. Note the almost face-on case has a pronounced  $10 \mu\text{m}$  silicate feature, while for the almost edge-on case the silicate feature has disappeared due to the absorption of the bulk of the disc.

#### 3.3 Fulcrum wavelength as a function of inner rim temperature, $T_{\text{rim}}$

Figure 7 shows the effect of varying the temperature of the inner puffed rim for a fixed stellar temperature on  $\lambda_f$  as a function of disc inclination. For a given inclination, as one increases the temperature of the inner rim,  $\lambda_f$ . For inner rim temperatures between  $1,250$  and  $2,000\text{K}$ ,  $9.2 \mu\text{m} > \lambda_f > 7.4 \mu\text{m}$ .

It is possible that some cTTs will have more refractory dust species located in the inner region of the disc (Dullemond & Monnier 2010) and that this will lead to a higher  $T_{\text{sub}}$ . It's also possible that as the disc evolves, the inner disc truncates and the disc inner rim will be located further out at larger radii and lower temperatures.

If the inner wall rim moves outwards and is cooler, then the inner wall component of the SED will move closer to the silicate feature. If the inner wall rim moves inwards and is warmer, then inner wall component will move to shorter  $\lambda$  and away from the silicate feature. This should cause the intersection of these two components of the SED - which will be at approximately the fulcrum wavelength - to move towards longer or shorter wavelengths respectively. This hypothesis was tested by running simulations for a fixed  $T_{\text{eff}} = 5,700$  K, but in which the temperature of the inner wall ( $T_{\text{rim}}$ ) is varied between  $1,000$  K and  $2,000$  K. Figure 7 depicts the results of these simulations.

We see, that the  $\lambda_f$  vs.  $i$  curves of fixed  $T_{\text{rim}}$  are convex, that they do not intersect, and that for  $T_{\text{rim}} < 1,500$  K have larger values of  $\lambda_f$  than on the fiducial curve, and for  $T_{\text{rim}} > 1,500$  K have smaller values of  $\lambda_f$  than on the fiducial curve.

#### 3.4 Gapped disc model

The disc surrounding LRL 31 has a gap from approximately  $1-15$  au (Espaillat et al. 2012; Pinilla et al. 2014). Figures 8 and 9 show the resulting SED for a range of puffed

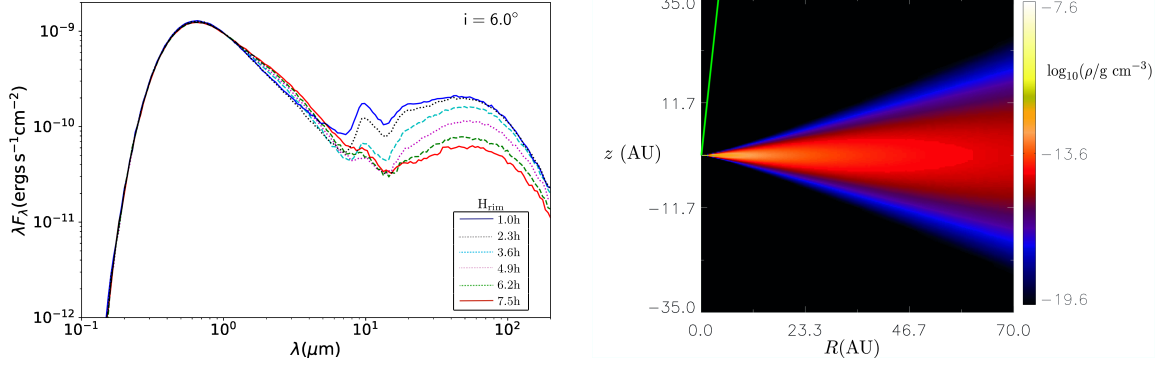


**Figure 3.** Left: The SEDs of LRL 31 for a variety of puffed inner rim heights,  $H_{\text{rim}}$ , for a near face-on system with inclination  $i = 6.0^\circ$ . Right: The modelled disc density with the line of sight superimposed in green (data from Sim.1)

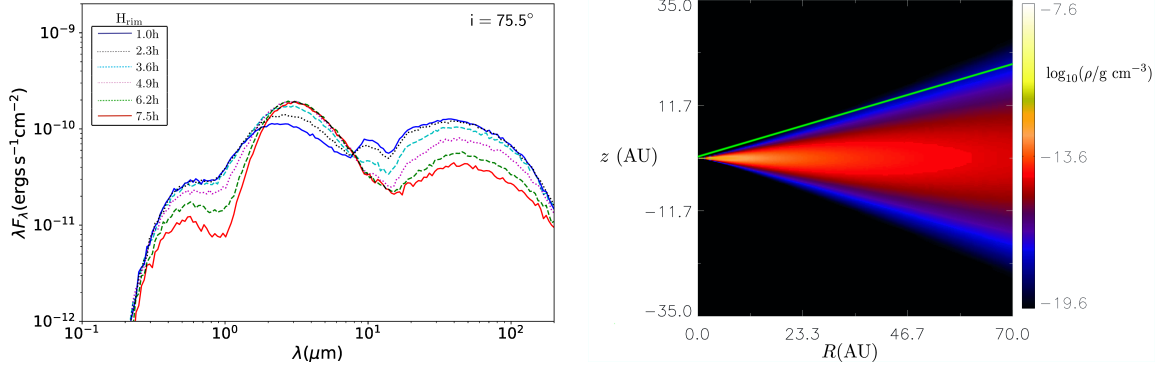


**Figure 4.** Same as Figure 3 for a near edge-on disc with inclination  $i = 75.5^\circ$  (Sim. 1)

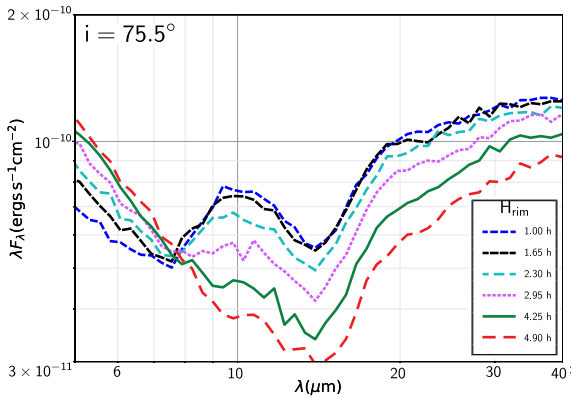


**Figure 5.** Mid-infrared portion of the SEDs of LRL 31, modelled as a full disc viewed near edge-on ( $i = 75.5^\circ$ ), for a range of  $H_{\text{rim}}$  values with a fulcrum point near  $7.7\mu\text{m}$  (Sim.1)

rim-heights,  $H_{\text{rim}}$  when  $i = 75.5^\circ$ . Again, as displayed in Figures 10 (a), (b), (c) & (d), we find for  $i < 75^\circ$  there is see-saw behaviour in the SED as the inner rim height changes, however there is no single fulcrum point until  $i \approx 75^\circ$

Comparing the MIR portion of the SED for the gapped disc model (Figure 9) to the same wavelength range of the full disc model (Figure 5) and the observational data (Figure

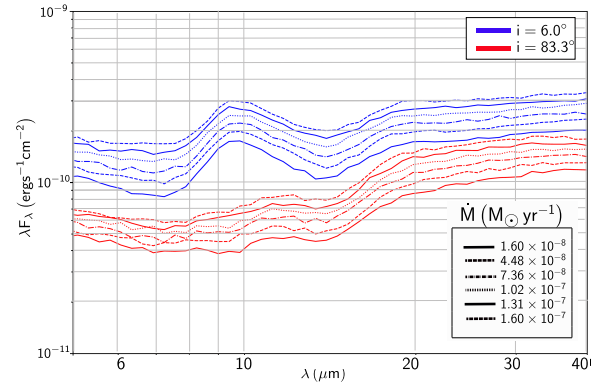


**Figure 6.** MIR SED of LRL 31 as a function of the mass accretion rate,  $\dot{M}$ , for an almost face-on (blue) and edge-on (red) disc (Sim. 2).

2) we note that the addition of the gap has the effect of: (i) moving  $\lambda_f$  from  $7.7\mu\text{m}$  to  $7.9\mu\text{m}$ , closer to the observed value of  $8.5\mu\text{m}$ ; moving the silicate peak in the SED from  $\approx 10\mu\text{m}$  to  $11.2\mu\text{m}$  which is close to the observed value of  $11\mu\text{m}$ , and finally moved the peak in the SED due to the outer wall from  $\approx 36\mu\text{m}$  to  $\approx 20\mu\text{m}$ , which is closer to the observed position of  $\approx 23.8\mu\text{m}$ .

Comparing the SEDs in Figures. 4 and 8, we note that

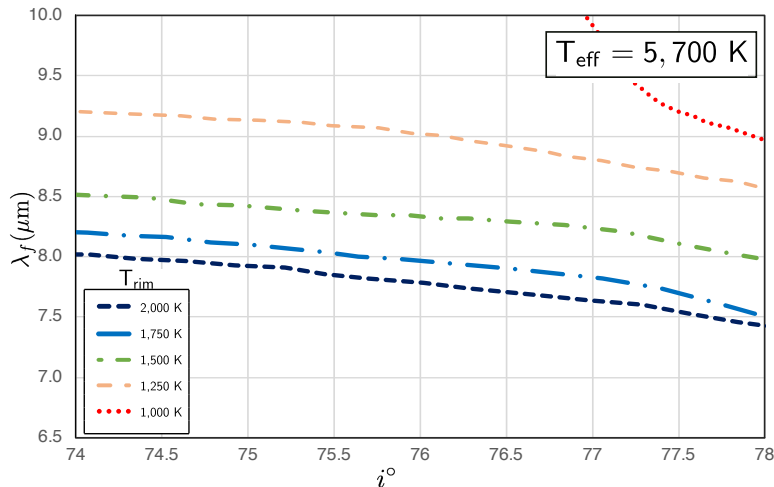


**Figure 7.** Fulcrum wavelength  $\lambda_f$  as a function of  $T_{\text{rim}}$  for  $T_{\text{eff}} = 5,700$  K, (Sim. 3)

$\lambda_f \approx 8\mu\text{m}$  does not change significantly between the full and gapped case, and that the general shape of the SEDs are very similar but that the peak in the curve beyond the silicate feature is slightly more pronounced for the gapped disc. In the right hand pane of Figure 8 which displays the density distribution, we see that exterior to the gap, the disc profile flares to form an outer wall and it is the additional flux from this cooler, outer wall that enhances the flux near  $20\mu\text{m}$ . The presence of a 14 au gap in the inner disc improves the match between the simulated SED and that arising from observations.

### 3.5 Varying the disc density profile

In simulations 5 and 6 we vary the exponents  $\alpha$  and  $\beta$ . Figure 11(a) shows the fulcrum wavelength as a function of the radial density exponent  $\alpha$  for a disc inclination of  $75.5^\circ$ . The fiducial value of  $\alpha = 2.25$  is varied between 2.0 and 2.5, which results in variations in  $\lambda_f$  between  $7.9\mu\text{m} < \lambda_f < 8.8\mu\text{m}$ .

Figure 11(b) shows significant variation in  $\lambda_f$  ( $28\mu\text{m} > \lambda_f > 7\mu\text{m}$ ) as the vertical disc exponent  $\beta$  varies between 1.0 and 1.3 (where the fiducial value is  $\beta = 1.25$ ). The value of  $\lambda_f$  is very sensitive to the degree to which disc flares, with flatter disc profiles moving  $\lambda_f$  to longer wavelengths.

## 4 DISCUSSION

### 4.1 Factors determining the presence of a $\lambda_f$

The primary goal of this work was to determine which parameters contribute to the presence of a unique fulcrum wavelength in the SED of this object. From the observations depicted in Figure 2, we note that the MIR flux varies substantially even within a week (between 9<sup>th</sup> and 16<sup>th</sup> October 2007). Therefore, only quantities capable of varying substantially on time scales as short as a week can be considered as a potential cause of the see-saw behaviour. Of the parameters varied in simulation, only the rim-height and the disc accretion rate can alter substantially on this timescale. Furthermore, the results of our simulations suggest that it is

variations in the inner rim height, for highly inclined discs, that principally contributes to the existence of a unique fulcrum wavelength, not the disc accretion rate. This connection between high disc inclination and the presence of a fulcrum point has not previously been identified.

Other than that it is high, the inclination  $i$  of the disc of LRL 31 is poorly constrained by observation to lie between  $70-85^\circ$ . So in our first set of simulations we swept over both rim height and inclination. For low to moderate inclinations the disc does not obscure the star and the stellar flux should remain constant.

As the rim height is increased, the flux intercepted by the inner disc wall from the star will increase nearly linearly with its height. If we also assume that the inner rim wall is optically thick, then, if the wall is at temperature  $T_{\text{sub}}$ , the flux from the wall will have the form of a blackbody of temperature  $T_{\text{sub}}$ . As the height of the rim increases the radius of the shadow on the disc lengthens and the temperature of the portion of the disc in shadow drops. This reduces the amount of longer wavelength radiation irradiated by the shadowed disc and causes the longer wavelength portion of the SED to pivot downwards to the right as the rim height increases. The  $10\mu\text{m}$  silicate feature will be in emission. The form of the SED predicted by these qualitative arguments agrees with the results of the simulations for small inclination ( $i = 6^\circ$ ) seen in Figures 3 and 10. Note that for this small angle of inclination there is no single  $\lambda_f$  but a set of crossing points located between 5 and  $10\mu\text{m}$ .

For high inclinations, as the inner rim height increases the line of sight intersects the puffed inner rim and the stellar photosphere starts to be obscured. The contribution of the photosphere to the total SED quickly falls away, with the emission peak in the SED near  $3\mu\text{m}$  due to the enlarged inner rim becomes much more prominent and the shadow cast on the disc exterior to the inner rim causes less flux to be emitted. As the rim height increases, the line of sight intercepts a greater density of dust and the  $10\mu\text{m}$  silicate feature moves from emission almost to absorption - see Figures 4 and 10. Near  $i = 74^\circ$  the line of sight intersects the surface of the disc and it is only at that point that a single



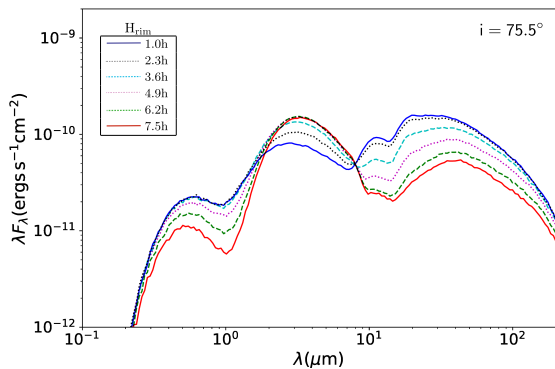


**Figure 8.** SEDs of LRL 31 modelled with a gap between 1-15 au with a viewing angle of  $i = 75.5^\circ$  (Sim. 4)

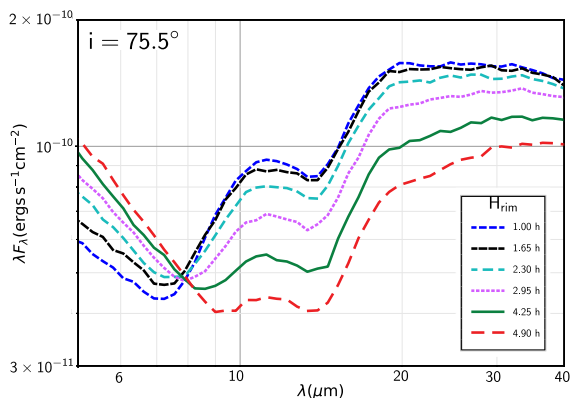
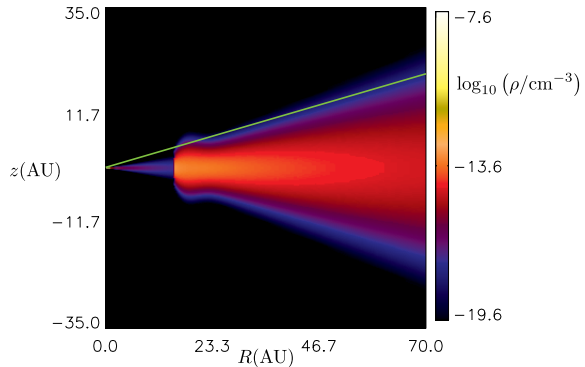


**Figure 9.** Same as Figure 5 with the disc modelled with a gap between 1-15 au and displaying a fulcrum point of  $7.9\mu\text{m}$  (Sim. 4).

$\lambda_f$  emerges (Figure 10). For  $74^\circ < i < 82^\circ$  there is a single  $\lambda_f$ , for  $i > 82^\circ$  the results of the simulations are noisy and it is difficult to clearly identify  $\lambda_f$ .

Crapsi et al. (2008) and Whitney et al. (2003a) have noted that for high inclinations, where the stellar source is observed through the bulk of the disc, the SED of class II YSOs become difficult to distinguish from that of class I YSOs. Class I YSOs typically have a double humped SED with the shorter wavelength peak due to the stellar object viewed at high extinction and a second longer wavelength peak due to the envelope. We found that our simulated SEDs began to take on this form at  $i \approx 82^\circ$ .

If it is assumed that the inclinations of discs of this class of MIR variables are uniformly distributed between  $0^\circ$  and  $90^\circ$  then we can make a very rough, first estimate of the fraction of stars in this class that have a fulcrum point. This fraction should equal the range of inclinations for which the objects will be observed to have a fulcrum point divided by the range of inclinations for which the SED has the unambiguous form associated with a class II YSO. Extrapolating from our simulations of LRL 31 we find:  $f = \frac{82^\circ - 74^\circ}{82^\circ} \approx 0.1$ . That is, about 10% of cTTs similar to LRL 31 would appear to an observer to have a fulcrum point.

## 4.2 The link between $\lambda_f$ and disc structure

The second goal of this study was to determine how the disc structure influences  $\lambda_f$  and the position of the fulcrum point relative to the  $10\mu\text{m}$  silicate feature. A number of the MIR variable cTTs studied in Espaillat et al. (2011) have  $\lambda_f > 10\mu\text{m}$  and so we explore whether our simulations can shed some light on which physical parameters may cause this shift.

Variations in the dust sublimation temperature  $T_{\text{sub}}$  or the dust sublimation radius  $R_{\text{sub}}$ , cause a small variation in  $\lambda_f$  for high disc inclinations. We show that the smaller  $T_{\text{sub}}$ , the larger  $R_{\text{sub}}$  and the larger  $\lambda_f$  (see Figure 7). However, it is possible that some other physical mechanism could lead to the inner rim of the disc being eroded, leading to a larger  $R_{\text{rim}}$  (such as the presence of a companion interior to the dust sublimation radius Larwood & Papaloizou (1997)). If this was the case, our simulations suggest that this could lead to  $\lambda_f > 10\mu\text{m}$ .

Indeed, there is indirect evidence from ALMA and VLA observations that planetary companions have carved gaps in the inner disc of the transition disc object GM Aur giving the appearance of an enlarged inner cavity (Macías et al. 2018).

While SED modelling by Espaillat et al. (2012) and Pinilla et al. (2014) suggests LRL 31 hosts a 14 au gap in the inner disc, our simulations show that a gap does not produce a significant change in  $\lambda_f$  in our simulations. On that basis we would not expect gaps of smaller width to significantly effect the value of  $\lambda_f$ . This raises the question of whether there is any observational evidence for YSOs with full discs, i.e. discs with no gaps, exhibiting this see-saw behaviour. Flaherty et al. (2012) and Espaillat et al. (2012) identified LRL 2 as a full disc YSO with a SED pivoting in the MIR. Espaillat et al. (2011) published Spitzer observations of RY Tau showing that it has a pivoting SED while Garufi et al. (2019) has identified it as a full or near full-disc object. Espaillat et al. (2011) also claimed that the SED of the YSO ISO 52 is best explained by a full disc.

Our simulations suggest that the flaring parameter  $\beta$  is important in determining the fulcrum wavelength  $\lambda_f$ . Semi-analytic, accretion disc models such as those developed by Kenyon & Hartmann (1987) and Chiang & Goldreich (1997) place constraints on the value of the flaring exponent  $\beta$  for

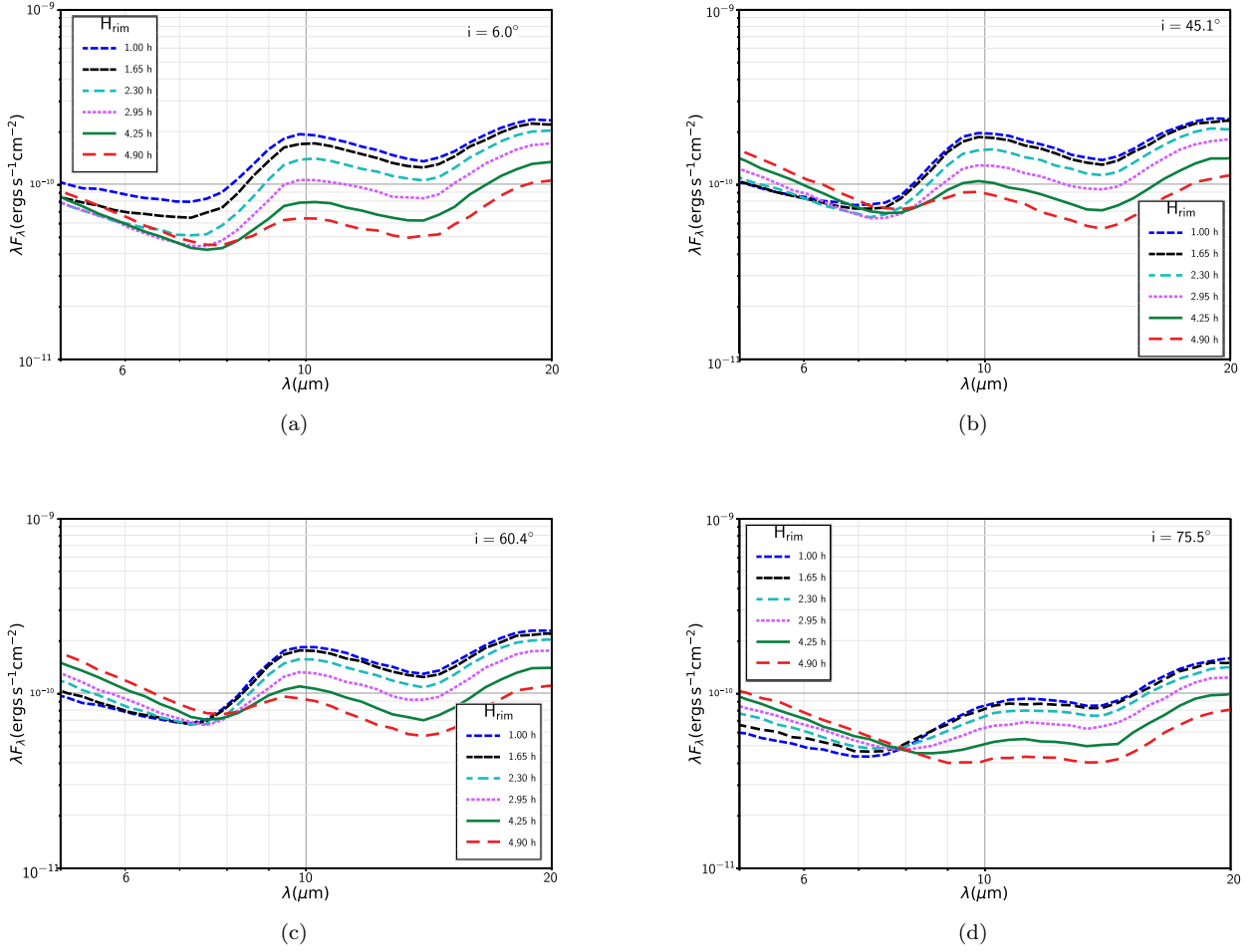


**Figure 10.** MIR portion, for a gapped disc (gap 1 - 15 au), of the SED for four inclinations: (a)  $i = 6.0^\circ$ ; (b)  $i = 45.1^\circ$ ; (c)  $i = 60.4^\circ$ ; and (d)  $i = 75.5^\circ$  for each of six puffed rim heights ( $1h < H_{\text{rim}} < 4.9h$ ). Note how the intersections of the curves move long-wards in wavelength as  $i$  increases and how the flux does not decrease substantially until the line of sight begins to intersect the disc ( $i > 70^\circ$ ).

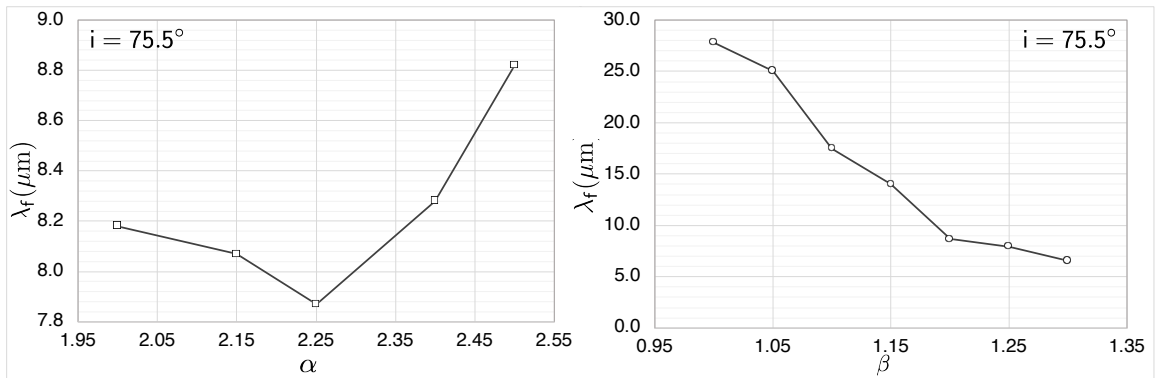


**Figure 11.** Variation in the fulcrum wavelength,  $\lambda_f$ , as (a): A function of the radial density exponent  $\alpha$  (Sim. 5), and (b) the vertical density exponent  $\beta$  (Sim. 6) for a disc inclination  $i = 75.5^\circ$ .

**Table 6.** Values of the flaring exponent  $\beta$  obtained from observations of a selection of T Tauri (cTTs) and Herbig Ae /Be (HAe/Be) stars

Object	$\beta$	Type	Ref.
MWC 325	$0.85 \pm 0.13$	HAe/Be	[4]
RXJ 1615	$1.116 \pm 0.095$	cTTs	[1]
HD 102964	$1.26 \pm 0.05$	HAe/Be	[2]
AB Aurigæ	$1.27 \pm 0.025$	HAe/Be	[5]
IM Lup	$1.271 \pm 0.197$	cTTs	[1]
ESO H $\alpha$ 569	1.29	cTTs	[3]
V4046 Sgr	$1.605 \pm 0.132$	cTTs	[1]
UX Ori	$1.79 \pm 0.12$	HAe/Be	[6]

[1] Avenhaus et al. (2018), [2] Lagage et al. (2006), [3] Wolff et al. (2017), [4] Ragland et al. (2012), [5] di Folco et al. (2009), [6] Kreplin et al. (2016)

passive, flaring discs (that is, for those discs in which viscous dissipation is not a significant source of energy, and for which the central star is visible from the surface of the entire disc). For  $\beta < 1.0$  the outer disc is self-shadowed by the inner disc (i.e. it does not flare), while  $\beta = 1$  represents a linear disc. Kenyon & Hartmann (1987) derived a minimum value of  $\beta = 1.125$  for a thin disc and a maximum value, (for a flared disc) of  $\beta = 1.25$ . Chiang & Goldreich (1997) derived a maximum value of  $\beta = 1\frac{2}{7} \approx 1.29$ . Dullemond et al. (2001) demonstrated that the presence of an inner disc cavity and the shadow of a puffed inner rim on the outer disc could explain the presence of a NIR bump in the SED of HAeBes, while in later papers (Dullemond & Dominik 2004; Isella & Natta 2005; van Boekel et al. 2005), the effects of dust-settling and a puffed, but curved inner rim on the flaring of the outer disc and the shadow cast upon it were further investigated. However, these later researches did not alter the limits on  $\beta$  for the outer disc established in the earlier work.

The recent development of new instruments capable of spatially resolving nearby discs in the infrared has enabled observations which have allowed the direct calculation of  $\beta$ . Table 6 shows values of  $\beta$  derived from observations of accretion discs around a selection of cTTs and HAe/Bes (Avenhaus et al. 2018; Lagage et al. 2006; di Folco et al. 2009; Kreplin et al. 2016; Ragland et al. 2012; Wolff et al. 2017). Resolved scattered light imaging and or otherwise observationally constrained SED modelling was used to determine  $\beta$ . These values range from the substantially self-shadowed (MWC 325,  $\beta = 0.85$ ) to the surprisingly flared (UX Ori,  $\beta = 1.79$ ). However, it should be noted that values of  $\beta$  listed in Table 6, cannot be easily compared with each other as the instruments used to make these measurements sample very different wavelength regions and hence different depths in and radii of their respective discs.

The range of  $\beta$  used in our simulations is a subset of these values. Our simulations indicate that the value of  $\lambda_f$  is very sensitive to the value of the flaring exponent  $\beta$ , but much less so to the radial exponent  $\alpha$ . For discs that are flatter than the fiducial disc ( $\beta < 1.25$ ),  $\lambda_f > 8\mu\text{m}$  and for discs with  $\beta < 1.20$ ,  $\lambda_f > 10\mu\text{m}$ . That is, for flatter discs the fulcrum point lies beyond the silicate feature.

Observations suggest that the surface densities of protoplanetary discs vary approximately as a power law in the

inverse cylindrical radius  $1/R$  with a positive exponent  $p$ . If the 3D-parametric density equation 1 is integrated over all  $z$  to obtain the surface density an identical expression is obtained provided  $p = (\alpha - \beta)$ . Integrating the surface density over  $R$  yields the disc mass and this additional constraint ensures that  $p < 2$ . Furthermore, the density of a protoplanetary disc generally decreases with radius ( $p > 0$ ), hence  $0 < p < 2$ .

For the minimum mass solar nebula Weidenschilling (1977) and Hayashi (1981) both infer  $p = 1.5$ . In a series of papers D’Alessio et al. (1998, 1999, 2001) showed that for an externally irradiated, passive disc in hydrostatic equilibrium  $p \approx 1$ . Hughes et al. (2008) fitted millimetre continuum emissions from four nearby disc systems using both the truncated power-law and exponentially tapered disc surface density models and found values of  $p \approx \gamma = [0.7, 1.3]$  while Andrews et al. (2009, 2010), modelling discs in Ophiuchus using the exponentially tapered model, found  $p \approx \gamma = 0.9 \pm 0.2$ .

If we fix  $\alpha = 2.25$ , which is consistent with the hydrostatic calculations of D’Alessio et al. (1999) and which was used in modelling T Tauri stars with flared discs by Wood et al. (2002); Whitney et al. (2003b) and Whitney et al. (2013), then for  $\beta = [1.0, 1.3]$ ,  $p = [1.25, 0.95]$  which falls within the range of these values.

The YSO’s SED can be approximately decomposed into components due to: the star, the inner rim, the dust feature and the outer disc. The star and inner rim contribution are largely unchanged by variations in the disk flaring parameter  $\beta$ . The  $10\mu\text{m}$  dust feature will be unaffected in position, but may vary somewhat in magnitude. The component of the SED due to the outer disc however will be affected by the value of the flaring exponent  $\beta$ . For a flatter disc, the shadow of the puffed inner rim will extend further radially and the stretched black body produced by the outer disc’s re-irradiation of the incoming stellar radiation will move towards longer wavelengths. For a significantly flared disc, the shadow cast by the inner rim will be truncated closer to the star as the disc rises out of the shadow of the puffed rim more quickly. Overall, the disk with a greater  $\beta$  will intercept more radiation closer to the star and this will give rise to a more compressed outer disc SED component with a peak located at somewhat shorter wavelengths. If the inner, puffed rim height is varied this variation in  $\beta$  should cause the SED’s of flatter discs to pivot at longer wavelengths than is the case for more flared discs.

In summary, the presence of a fulcrum point in the SED is suggestive of a high inclination of the disc to the line of sight, while the position of the fulcrum point relative to the  $10\mu\text{m}$  silicate feature (either in emission or absorption) may be predictive of how much the disc flares.

## 5 CONCLUSION

Our radiative transfer simulation studies of LRL 31 using Hochunk3D have established its accretion disc has a fluctuating inner rim height, certainly within the range  $h < H_{\text{rim}} < 6.0h$ . Furthermore they have shown that:

- (i) The presence of a single fulcrum point  $\lambda_f$  depends upon the disc being highly inclined ( $> 70^\circ$ )
- (ii) The inclination cannot be so high that the  $10\mu\text{m}$  silicate feature goes into absorption ( $i < 85$  degrees)

(iii) For our gapped disc model, with a gap between 1–15 au and with density profile exponents  $\alpha = 2.25$  and  $\beta = 1.25$ , we found a single fulcrum point with  $\lambda_f \approx 8.0\mu\text{m}$  near the observed value of  $\lambda_f = 8.5\mu\text{m}$

(iv) Altering the disc accretion rate by itself cannot explain the see-saw variations in flux

(v) The presence or absence of a gap in the disc between 1 and 15 au does not have a strong influence on the position of the fulcrum point – although it does improve the agreement between the simulations and the observations.

(vi) The position of the fulcrum point is most strongly influenced by  $\beta$  with variations in other parameters not having a strong effect

(vii) Keeping all else fixed, as we reduce the value of  $\beta$  below the fiducial value of 1.25, the fulcrum point moves to ever longer wavelengths. For  $\beta$  small enough,  $\lambda_f > 10\mu\text{m}$ , that is it lies beyond the silicate feature in the SED.

## ACKNOWLEDGEMENTS

This work was performed on the gSTAR national facility at Swinburne University of Technology. gSTAR is funded by Swinburne and the Australian Government's Education Investment Fund.

GRB acknowledges the support of a Swinburne University Postgraduate Research Award (SUPRA).

## REFERENCES

- ALMA Partnership et al., 2015, *ApJ*, **808**, L3  
 Ábrahám P., et al., 2009, *Nature*, **459**, 224  
 Alexander R. D., Clarke C. J., Pringle J. E., 2006a, *MNRAS*, **369**, 216  
 Alexander R. D., Clarke C. J., Pringle J. E., 2006b, *MNRAS*, **369**, 229  
 Andrews S. M., Wilner D. J., Hughes A. M., Qi C., Dullemond C. P., 2009, *ApJ*, **700**, 1502  
 Andrews S. M., Wilner D. J., Hughes A. M., Qi C., Dullemond C. P., 2010, *ApJ*, **723**, 1241  
 Ansdell M., Gaidos E., Williams J. P., Kennedy G., Wyatt M. C., LaCourse D. M., Jacobs T. L., Mann A. W., 2016a, *MNRAS*, **462**, L101  
 Ansdell M., et al., 2016b, *ApJ*, **828**, 46  
 Avenhaus H., et al., 2018, *ApJ*, **863**, 44  
 Beckwith S. V. W., Sargent A. I., 1991, *ApJ*, **381**, 250  
 Beckwith S. V. W., Sargent A. I., Chini R. S., Guesten R., 1990, *AJ*, **99**, 924  
 Bouvier J., et al., 1999, *A&A*, **349**, 619  
 Bouvier J., Alencar S. H. P., Harries T. J., Johns-Krull C. M., Romanova M. M., 2007, in Reipurth B., Jewitt D., Keil K., eds, *Protostars and Planets V*. p. 479 ([arXiv:astro-ph/0603498](#))  
 Chiang E. I., Goldreich P., 1997, *ApJ*, **490**, 368  
 Cody A. M., et al., 2014, *AJ*, **147**, 82  
 Crapsi A., van Dishoeck E. F., Hogerheijde M. R., Pontoppidan K. M., Dullemond C. P., 2008, *A&A*, **486**, 245  
 D'Alessio P., Cantó J., Calvet N., Lizano S., 1998, *ApJ*, **500**, 411  
 D'Alessio P., Calvet N., Hartmann L., Lizano S., Cantó J., 1999, *ApJ*, **527**, 893  
 D'Alessio P., Calvet N., Hartmann L., 2001, *ApJ*, **553**, 321  
 Dong R., 2015, *ApJ*, **810**, 6  
 Dullemond C. P., Dominik C., 2004, *A&A*, **417**, 159  
 Dullemond C., Monnier J., 2010, *ARA&A*, **48**, 205  
 Dullemond C. P., Dominik C., Natta A., 2001, *ApJ*, **560**, 957  
 Espaillat C., et al., 2010, *ApJ*, **717**, 441  
 Espaillat C., Furlan E., D'Alessio P., Sargent B., Nagel E., Calvet N., Watson D. M., Muzerolle J., 2011, *ApJ*, **728**, 49  
 Espaillat C., et al., 2012, *ApJ*, **747**, 103  
 Flaherty K. M., Muzerolle J., 2010, *ApJ*, **719**, 1733  
 Flaherty K. M., Muzerolle J., Rieke G., Gutermuth R., Balog Z., Herbst W., Megeath S. T., Kun M., 2011, *ApJ*, **732**, 83  
 Flaherty K. M., Muzerolle J., Rieke G., Gutermuth R., Balog Z., Herbst W., Megeath S. T., Kun M., 2012, *ApJ*, **748**, 71  
 Flaherty K. M., DeMarchi L., Muzerolle J., Balog Z., Herbst W., Megeath S. T., Furlan E., Gutermuth R., 2016, *ApJ*, **833**, 104  
 Garufi A., et al., 2019, arXiv e-prints, p. [arXiv:1906.06910](#)  
 Hayashi C., 1981, *Progress of Theoretical Physics Supplement*, **70**, 35  
 Hughes A. M., Wilner D. J., Qi C., Hogerheijde M. R., 2008, *ApJ*, **678**, 1119  
 Ireland M. J., Kraus A. L., 2008, *ApJ*, **678**, L59  
 Isella A., Natta A., 2005, *A&A*, **438**, 899  
 Kenyon S. J., Hartmann L., 1987, *ApJ*, **323**, 714  
 Kenyon S. J., Hartmann L., 1995, *Ap&SS*, **101**, 117  
 Kim S.-H., Martin P. G., Hendry P. D., 1994, *ApJ*, **422**, 164  
 Koepferl C. M., Ercolano B., Dale J., Teixeira P. S., Ratzka T., Spezzi L., 2013, *MNRAS*, **428**, 3327  
 Konigl A., Pudritz R. E., 2000, in Mannings V., Boss A. P., Russell S. S., eds, *Protostars and Planets IV*. p. 759 ([arXiv:astro-ph/9903168](#))  
 Königl A., Salmeron R., Wardle M., 2010, *MNRAS*, **401**, 479  
 Kreplin A., Madlener D., Chen L., Weigelt G., Kraus S., Grinin V., Tambovtseva L., Kishimoto M., 2016, *A&A*, **590**, A96  
 Lagage P.-O., et al., 2006, *Science*, **314**, 621  
 Lai D., Zhang H., 2008, *ApJ*, **683**, 949  
 Larwood J. D., Papaloizou J. C. B., 1997, *MNRAS*, **285**, 288  
 Liffman K., Maddison S., Bryan G., 2019, *Infrared Variability due to Magnetic Pressure Driven Jets, Dust Ejection and Quasi-Puffed-Up Inner Rims*, submitted to *MNRAS*  
 Luhman K. L., Stauffer J. R., Muench A. A., Rieke G. H., Lada E. A., Bouvier J., Lada C. J., 2003, *ApJ*, **593**, 1093  
 Lynden-Bell D., Pringle J. E., 1974, *MNRAS*, **168**, 603  
 Macías E., et al., 2018, *ApJ*, **865**, 37  
 Morales-Calderón M., et al., 2011, *ApJ*, **733**, 50  
 Muzerolle J., Hartmann L., Calvet N., 1998, *AJ*, **116**, 2965  
 Muzerolle J., et al., 2009, *ApJ*, **704**, L15  
 Natta A., Prusti T., Neri R., Wooden D., Grinin V. P., Mannings V., 2001, *A&A*, **371**, 186  
 Pinilla P., et al., 2014, *A&A*, **564**, A51  
 Pringle J. E., 1981, *ARA&A*, **19**, 137  
 Ragland S., et al., 2012, *ApJ*, **746**, 126  
 Rebull L. M., et al., 2015, *AJ*, **150**, 175  
 Weidenschilling S. J., 1977, *Ap&SS*, **51**, 153  
 Whitney B. A., Wood K., Bjorkman J. E., Wolff M. J., 2003a, *ApJ*, **591**, 1049  
 Whitney B. A., Wood K., Bjorkman J. E., Cohen M., 2003b, *The Astrophysical Journal*, **598**, 1079  
 Whitney B. A., Wood K., Bjorkman J. E., Cohen M., 2003c, *ApJ*, **598**, 1079  
 Whitney B. A., Indebetouw R., Bjorkman J. E., Wood K., 2004, *ApJ*, **617**, 1177  
 Whitney B. A., Robitaille T. P., Bjorkman J. E., Dong R., Wolff M. J., Wood K., Honor J., 2013, *The Astrophysical Journal Supplement Series*, **207**, 30  
 Wolff S. G., et al., 2017, *ApJ*, **851**, 56  
 Wood K., Wolff M. J., Bjorkman J. E., Whitney B., 2002, *ApJ*, **564**, 887  
 di Folco E., Dutrey A., Chesneau O., Wolf S., Schegerer A., Leinert C., Lopez B., 2009, *A&A*, **500**, 1065  
 van Boekel R., Dullemond C. P., Dominik C., 2005, *A&A*, **441**, 563

This paper has been typeset from a  $\text{\TeX/L\AA\TeX}$  file prepared by the author.